Journal of Colloid and Interface Science 601 (2021) 124–132

Contents lists available at ScienceDirect

Journal of Colloid and Interface Science

journal homepage: www.elsevier.com/locate/jcis

Regular Article

Absorption kinetics of nanocellulose foams: Effect of ionic strength and surface charge

Laila Hossain, Emily Eastman, Monica De Rango, Vikram Singh Raghuwanshi, Joanne Tanner, Gil Garnier *

Bioresource Processing Research Institute of Australia (BioPRIA), Department of Chemical Engineering, Monash University, Clayton, VIC-3800, Australia

HIGHLIGHTS

- Nanocellulose foam absorption mechanism follows a three stages process.
- Absorption capacity is reduced as increases the ionic strength of the fluid.
- Foam structure homogeneity increases with fiber's surface charge.
- Absorption kinetics is tailored by controlling fiber's surface charge and foam pore size.

GRAPHICAL ABSTRACT

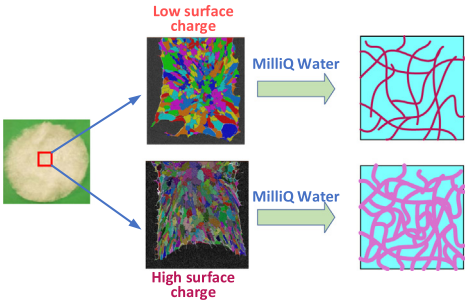

ARTICLE INFO

Article history:
Received 14 April 2021
Revised 13 May 2021
Accepted 15 May 2021
Available online 19 May 2021

Keywords:
Nanocellulose
Foam
Absorption
X-ray computed tomography
Structure
Wicking
Pore size

ABSTRACT

Hypothesis: The absorption capacity and kinetics of nanocellulose foams are controlled by the surface charge of the fibers, which affects swelling and determine the porosity and structure of the network.
Experiments: Absorption kinetics were quantified at time scales ranging from fractions of a second to minutes. The mass absorption rate as well as the area profile for the liquid stains were simultaneously measured.
Findings: The absorption profile followed a three-stage mechanism: wicking, transition and fiber swelling. Absorption of fluids differing in ionic strength revealed the critical role played by electrostatic forces. Nanocellulose foam absorption capacity is 25% higher for water than for 0.9 wt% NaCl solution. The absorption kinetics of nanocellulose foam are also tuneable by modulating the surface charge. High surface charge nanocellulose foams have slower absorption in water than their low surface charged analogues. This behaviour is driven by the lower pore sizes developed in high surface charge foams, as determined by X-ray CT. Small Angle X-ray Scattering revealed structural homogeneity of high surface charge foams upon absorption of water due to high fibrillation and fiber swelling.

1. Introduction

Superabsorbent polymers (SAPs) are three-dimensional, cross-linked, hydrophilic polymer networks capable of absorbing a large volume of water relative to their dry mass [1]. They are used extensively in personal hygiene products, diapers, agriculture, horticulture, biomedical applications, and food packaging [2,3]. However, most current commercial superabsorbents are based on sodium polyacrylate, a petrochemical-derived polymer which is non-degradable and non-renewable. Several renewable alternatives have been developed using cellulose, starch, gum, chitin and chitosan [4,5]. Among those, cellulose appears to be the most promising renewable SAPs feedstock due to its worldwide abundance, low cost and inherent biodegradability. Cellulose fiber production is also well known and established on a

* Corresponding author.
E-mail address: gil.garnier@monash.edu (G. Garnier).

https://doi.org/10.1016/j.jcis.2021.05.092
0021-9797/

commercial scale. Further processing of commercial cellulose fibers into carboxylated, nano-sized fibrils, followed by lyophilization, produces nanocellulose foams with superabsorbent properties [6,7].

Nanocellulose foam material is comprised of entangled fibers which create the pores. When in contact with water, these pores and fibers accommodate water. There are literatures on fluid absorption in paper like swelling media where absorption occurs by a combination of wicking and fiber swelling [8,9]. Wicking is the rapid flow of a fluid into the pores that exist between fibers, and is driven by capillary forces. This capillary action occurs when the cohesive force between the fluid molecules and the solid fiber surface is greater than the cohesive force between fluid molecules themselves. Fiber swelling occurs at a lower length scale and involves diffusion of the fluid through the fibers themselves. A difference in osmotic pressure between the fibers and the bulk solution in the foam pores provides the driving force for fiber swelling [10]. Swelling of fibers results in partial filling of the interfiber pore spaces and disruption of intrafiber hydrogen bonds between fibers, causing an overall expansion of the material [11].

Via the above mechanisms, nanocellulose foams can and do exhibit superabsorbent properties comparable to commercial SAPs. However, their absorption characteristics depend on a number of variables. For example, foams made with cellulose fibers that have residual associated lignin generally have a lower absorption capacity compared to analogous foams made with pure cellulose fibers due to the hydrophobic nature of lignin [12]. The ionic strength of the liquid to be absorbed can also affect absorption kinetics and capacity due to the influence of ionic strength of the bulk fluid on the osmotic pressure difference that controls fiber swelling. Other factors potentially affecting the superabsorbent properties of nanocellulose foams include the cellulose composition, cellulose surface charge, foam surface area, foam porosity, absorbate pH, absorbate temperature and absorbate composition [13].

There are many reports in the literature on the production of nanocellulose foams that claim or demonstrate superabsorbent properties [14–19]. Absorption kinetics have also been determined for various examples of nanocellulose foams at time scales ranging from minutes to days, depending on the saturation duration of the material under investigation [2,3,20]. However, no study has yet correlated or quantified the initial absorption rate or phases of the absorption mechanism with differences in either nanocellulose foam structure at the various critical length and time scales of interest, particularly for foams exhibiting rapid (second to minute-scale) absorption kinetics. Moreover, the effect of fiber surface charge and the absorbate solution ionic strength on nanocellulose-based SAPs absorption kinetics, both of which are critical to the tuning of these materials for specific applications, have not been rigorously quantified.

This study investigates the effect of the nanocellulose fiber surface charge on the structure, absorption kinetics, and absorption capacity of nanocellulose foams. Here we demonstrate for the first time that there are three distinct phases of absorption, and present the kinetics of these characteristic phases of fluid absorption in nanocellulose foams. The impact of the combination of different fiber surface charges and solution ionic strengths on this mechanism is also shown, using a 0.9 wt% NaCl solution, to represent the typical ionic strength of body fluids including blood, urine and sweat and demonstrate the suitability of these materials to replace petrochemical SAPs in common commercial applications

2. Experimental

2.1. Materials

Bleached Eucalyptus Kraft (BEK) pulp was used as supplied from Australian Paper, Maryvale. 2,2,6,6-Tetramethylpiperidine-1-oxyl (TEMPO), Hydrochloric acid (HCl), Sodium Periodate ($NaIO_4$), Sodium Hydroxide (NaOH) and Sodium Bromide (NaBr) were purchased from Sigma Aldrich. 12 w/v% Sodium Hypochlorite (NaClO) was bought from Thermo Fischer Scientific and used as supplied. Hydrochloric acid (HCl) and Sodium Hydroxide (NaOH) diluted for solutions as required.

2.2. Methods

2.2.1. TEMPO-mediated oxidation

The TEMPO-mediated oxidation process employed to produce low surface charged fibers was based on a previously developed method [21]. 100 g BEK pulp (dry weight basis) was suspended in 2500 mL water containing 0.4 g TEMPO and 2.5 g NaBr. The 12 w/v% NaClO solution was initially adjusted to pH 10 via addition of 36 w/v% HCl. 100 mL NaClO was added drop-wise to the suspension whilst stirring. The pH of the reaction was maintained at 10 through the addition of 0.5 M NaOH. The oxidation process was deemed to be complete when the pH change was negligible. The oxidized fibers were washed and vacuum filtered until neutral pH was achieved and stored at 4 °C. This preparation method produces oxidized fiber with a surface charge of 1.3 mmol carboxylate (COO^-) groups per gram fiber. Fiber produced by this method and foams produced from this fiber are referred to as low surface charge (LSC) in this work. The TEMPO-oxidized pulp was then dispersed in deionized water at a desired concentration. Fibrillation and hydrogel formation were accomplished through a high-pressure homogeniser at 1000 bar with two passes. Nanocellulose foams were prepared by spreading 30 g of gel in a 50 mm petri dish and freezing at −80 °C for 4 h. Once frozen, all samples were freeze-dried for 48 h.

2.2.2. One-shot TEMPO-periodate oxidation

The one-shot TEMPO-periodate oxidation process employed to produce high surface charged fibers was based on a previously developed method [22]. 25 g (dry weight basis) of BEK pulp were suspended in 1200 mL distilled water with 20 g NaBr, 13.5 g $NaIO_4$, and 2 g TEMPO. The outside of the reaction vessel was covered with aluminum foil to prevent photoinduced decomposition of periodate. 120 mL NaClO (12% v/v, pH adjusted to 10.5) was added dropwise under constant stirring. The pH of the reaction was maintained at 10.5 by adding 0.5 M NaOH. After 4 h, the oxidation reaction was stopped by quenching with 10 mL ethanol. The water-insoluble fraction was recovered by vacuum filtration and washed several times with distilled water until a neutral pH in the filtrate stream was achieved. The fibers were then freeze-dried for 48 h. This preparation method produces oxidized fiber with a surface charge of 1.89 mmol carboxylate (COO^-) groups per gram fiber. Fiber produced by this method and foams produced from this fiber are referred to as high surface charge (HSC) in this work.

2.2.3. Determination of solids concentration

The solids concentration of sample (i.e. hydrogel or pulp) was determined through oven drying using a previously developed method [13]. The initial weight (w_i) was recorded before the sample was placed in a ventilated oven at 105 °C for at least 4 h and the sample dried to a constant final weight, w_f. The solids content was determined by:

$$Solids\ content(\%) = \frac{w_f - w_i}{w_i} \times 100\% \quad (1)$$

2.2.4. Determination of carboxylate content

The carboxylate content of the nanocellulose fiber was determined via conductimetric titration using a previously developed method [13]. 0.2 g dry oxidized pulp was suspended in 40 mL deionized water. The sample pH was then lowered to pH 2.5–3 by adding 0.5 M HCl to ensure protonation of all carboxylate groups prior to the beginning of titration. Sample titration was initiated by the addition of 0.1 mL/min 0.1 M NaOH (Mettler Toledo T5 Titrator). The conductivity was monitored throughout the progress of the titration. The amount of carboxylate groups was calculated by:

$$Carboxylatecontent\left(\frac{mmol}{g}\right) = \frac{c(V_2 - V_1)}{w} \times 1000 \quad (2)$$

where the difference in V_2 and V_1 reflects the required amount, in litres, of titrant required to neutralize the carboxylic groups (plateau region of the titration curve), c is the NaOH concentration (mol/L), and w is the dry sample weight (g).

2.2.5. Micro-CT analysis

Micro-CT scanning was performed with a Phoenix Nanotom m (GE Sensing & Inspection Technologies GmbH, Wunstorf, Germany) operated using xs control and Phoenix datos|x acquisition software (both GE Sensing & Inspection Technologies).

Foam specimens were mounted on glass rods using a drop of hot glue to at base. The x-ray energy (20 kV and 400 μA) of scans and integration time for x-ray projections (2 s) was optimized to enhance contrast in the foam specimens, which exhibited a very low density relative to the surrounding air. Scans were run at a resolution of 8 μm collecting 1200 projections over a 125-minute period. Volume reconstruction of the micro-CT data was performed using Phoenix datos|x reconstruction software (GE Sensing & Inspection Technologies) applying a median filter and ROI filter during reconstruction. The data was exported as 16-bit volume files for analysis.

Analysis of reconstructed data was conducted using Avizo (Thermo Fisher Scientific). The foam structure was segmented using an interactive threshold and a sample mask created by closing and filling the structure. An inversion of the foam structure within the mask represents the pore space between the foam structure. The segmented volume and volume fraction of foam and pore space was then determined relative to the sample mask. Individual pores were segmented and the pore size distribution produced by labelling and separating the segmented pore space using a Chamfer algorithm, which is based on a watershed analysis of the data.

2.2.6. Absorption kinetics

The nanocellulose foam to be tested was cut into 2 cm × 2 cm samples using a laser cutter (EPILOG Laser). The edge of a sample was attached to a metal rod with superglue. The minimum amount of glue required to attach the sample to the rod was used to minimize interference with absorption experiments since the glue is hydrophobic. The rod with sample attached was hung from the hook on the bottom of a balance, so the nanocellulose foam sample was hanging above a reservoir of either deionized water or 0.9% NaCl solution on a height-adjustable stage. The balance was connected to a laptop via LabX Direct Balance Software to record the weight of the sample at specified time intervals. Three drops of food dye were mixed through the absorbate to provide greater contrast for image analysis. Care was taken to ensure the edge of the sample was parallel to the fluid surface so the entire edge will contact the fluid at the same time. This experimental set-up is shown in Fig. 1.

The pre-weighed sample was slowly lowered by adjusting the reservoir stage height. Care was taken to ensure that both the sample and the absorbate surface remained stationary while moving the stage. Once the edge of the sample was just touching the surface of the absorbate, height adjustment of the stage was stopped. After 5 min, the stage was moved downwards so that the sample was no longer touching the absorbate and the final weight of the saturated sample was recorded. This final weight was divided by the dry weight of the sample to give the weight of absorbate taken up per gram of dry nanocellulose sample.

This experiment was conducted in triplicate with 0.9% NaCl solution and in triplicate with water for vertical orientation of the sample in a controlled environment of 23 °C and 50% relative humidity. A video camera (FLIR Systems, Model: FL3-U3-13E4C-C: 1.3 MP, 60 FPS, e2v EV76C560, Color) was installed to capture images of each absorption trial. The images were converted to binary (black and white) in MATLAB, and the stained area of the sample in the image was used to calculate the area of absorption of the sample.

The results are reported as the average and standard deviation of the calculated absorption areas of the three replicates for each absorbate. The effects of buoyancy and surface tension have not been considered in this study.

2.2.7. Small angle X-ray scattering (SAXS)

Small angle X-ray Scattering (SAXS) experiments were conducted at the SAXS/WAXS beamline of the Australian Synchrotron with the assistance of Beamline Scientist Nigel Kirby. An X-ray energy of 12 KeV was used, and the samples were measured in the transmission mode. A 2D Pilatus detector was placed at the long distance of 7 m from the sample to cover a large size range. During measurements samples were first measured in the dried state and later measured as fully wetted with MilliQ water or 0.9% NaCl solution. A glassy carbon and silver behenate standards were used for the calibration. The in-house developed software Scatterbrain was used for data reduction and plotting of the 2D images.

3. Results

The absorption kinetics is measured in increments of 0.1 s for five minutes for nanocellulose foams made from fibers of two different surface charges of 1.3 mmol COO^-/g fiber and 1.89 mmol COO^-/g fiber produced from TEMPO and TEMPO-periodate oxidation, respectively. These foams are used separately to absorb MilliQ water and a saline solution (0.9 wt% NaCl). Continuous online image capturing and analysis are performed to quantify the absorption phases at complementary time scales.

3.1. Effect of liquid ionic strength

Fig. 2 illustrates the absorption profile of low surface charge (LSC) nanocellulose foam for MilliQ water and 0.9 wt% NaCl solution to quantify the effect of ionic absorbates on the absorption kinetics. The nanocellulose foam has a larger absorption capacity in water than in saline solution (Fig. 2). After 5 min, nanocellulose foam absorbed 81 g/g of MilliQ water versus 65 g/g for the NaCl solution. The initial kinetics of nanocellulose foam absorption were measured from the first 10 s (inset of Fig. 2). After 1 s, the difference in the amount of fluid absorbed is already significant, with 53 g/g of MilliQ water and 38 g/g of NaCl solution. Absorption of NaCl solution appears to be lower than that of MilliQ water due to Na^+ shielding the COO^- groups of the nanocellulose foam,

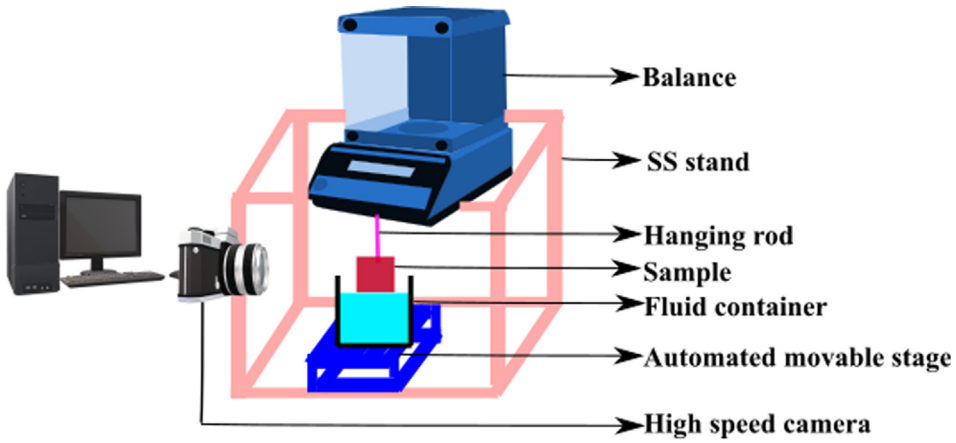

Fig. 1. Schematic diagram of the testing system to measure simultaneously the absorption kinetics of NC foam as well as the area of the liquid stain.

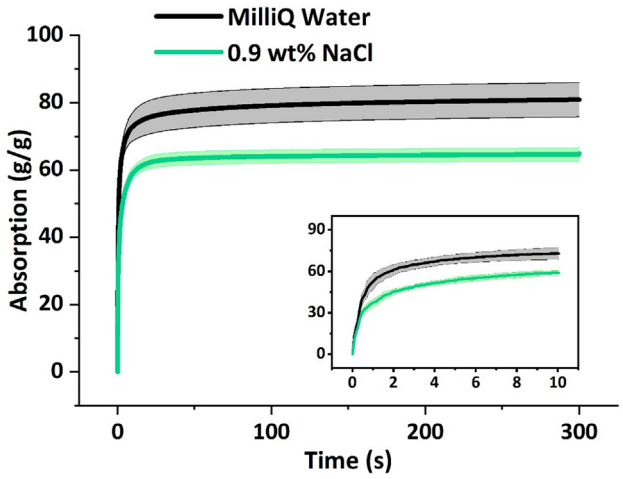

Fig. 2. Effect of liquid ionic strength on LSC nanocellulose foam absorption kinetics over a period of 5 min for MilliQ water and 0.9 wt% NaCl. The inset shows the effect of ionic strength over 10 s. The solid line represents the average result (n = 3), while the shaded zone indicates the range formed by one standard deviation.

decreasing its hydrophilicity and reducing the absorption capacity [23].

3.2. Effect of fiber surface charge

The impact of fiber surface charge on the absorption behavior of nanocellulose foam is measured using foams of two different charge densities: 1.3 mmol COO^-/g (low surface charge, LSC) and 1.89 mmol COO^-/g (high surface charge, HSC). The dimensions of these two different fibers are provided in Table 1. The high surface charge fibers are shorter and slightly thinner than the low surface charge fibers.

The effect of nanocellulose surface charge on absorption kinetics was assessed. Fig. 3 shows the absorption profiles of LSC and HSC foams for MilliQ water and 0.9 wt% NaCl at different time scales. HSC foam has a slower absorption kinetics than LSC at the short time scales (inset of Fig. 3A), but displays a slightly higher overall absorption capacity after 5 min (Fig. 3A).

SAXS scattering of the nanocellulose foams in their dry and wet forms was measured (Fig. 4). For the LSC foam, there are sharp boundaries due to aggregated fibers found under both dry and wet conditions. This means some structural heterogeneity caused by a lower fibrillation and lower fiber swelling in the dry and wet state, respectively. However, the HSC wet foam in MilliQ water does not show these sharp boundaries. The HSC foam has higher inter-fiber repulsion which results in a higher fibrillation as evidenced from the lower fiber diameter measured (Table 1). This higher fibrillation together with high fiber swelling lead to the structural homogeneity observed for the HSC samples in MilliQ water. However, when HSC foam is wetted with a saline solution, some sharp boundaries from aggregated fibers are formed. This indicates a reduced charge repulsion and fiber swelling due to the high ionic strength of the absorbate.

Table 1
Effect of oxidation on fiber dimension and charge [24].

Type of nanocellulose foam	Surface charge (mmol/g)	Fiber length (μm) × dia (nm)
TEMPO oxidized nanocellulose foam (LSC)	1.30	(>1) × (>5)
TEMPO-periodate oxidized nanocellulose foam (HSC)	1.89	(0.5) × (2–4)

3.3. Structural analysis by micro CT

Structural analysis of the nanocellulose foam samples was performed by X-ray Computed Tomography (CT). The three-dimensional separated pores for both LSC and HSC are shown in the videos provided in the supplementary section (V1_LSC and V2_HSC). Fig. 5 shows the 3D structures of the nanocellulose foams, the separated pore structure of the foams in the X-Z plane, and their pore size distributions. The HSC foam shows smaller pores than the LSC foam (Fig. 5E and F). The HSC foam has a higher frequency (~9000) of the smallest pore volumes (2×10^{-5} – 1×10^{-1} mm^3) compared to the LSC foam (~2000). The HSC foam is more homogeneous and denser, as shown by the 3D structure (Fig. 5 A-B), due to the smaller pore volumes relative to the LSC foam. The LSC has a wider range of pore size distribution, contributing to structural heterogeneity.

4. Discussion

4.1. Absorption mechanism of nanocellulose foam

The liquid absorption profiles of nanocellulose foams follow an exponential plateau relationship with time and demonstrate the three stages of absorption in nanocellulose foams: wicking, transition phase and fiber swelling. In this work, wicking corresponds well with the period of increasing absorption area as determined

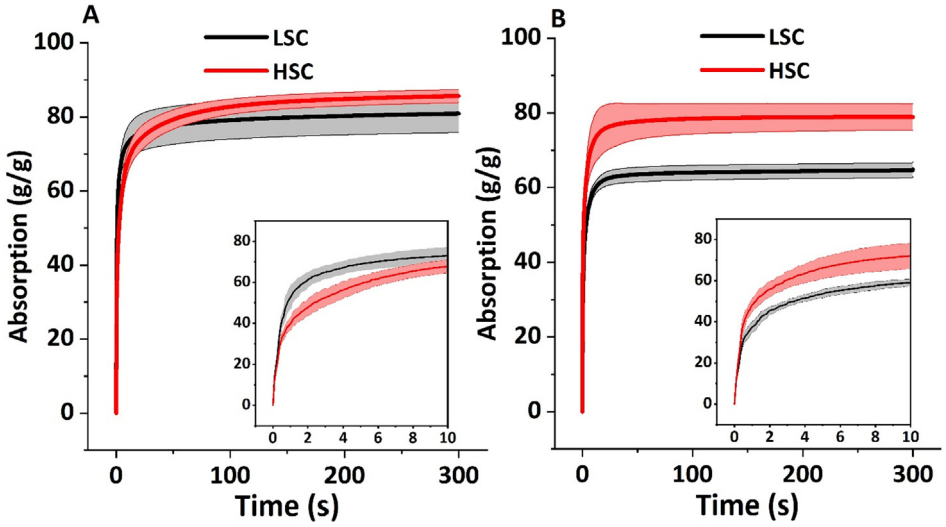

Fig. 3. Effect of low and high fiber surface charge on the absorption kinetics after 5 min for: (A) MilliQ water and (B) 0.9 wt% NaCl. The insets show the magnified graphs over a 10 s period. The solid line represents the average (n = 3), while the shaded zone indicates the range formed by one standard deviation.

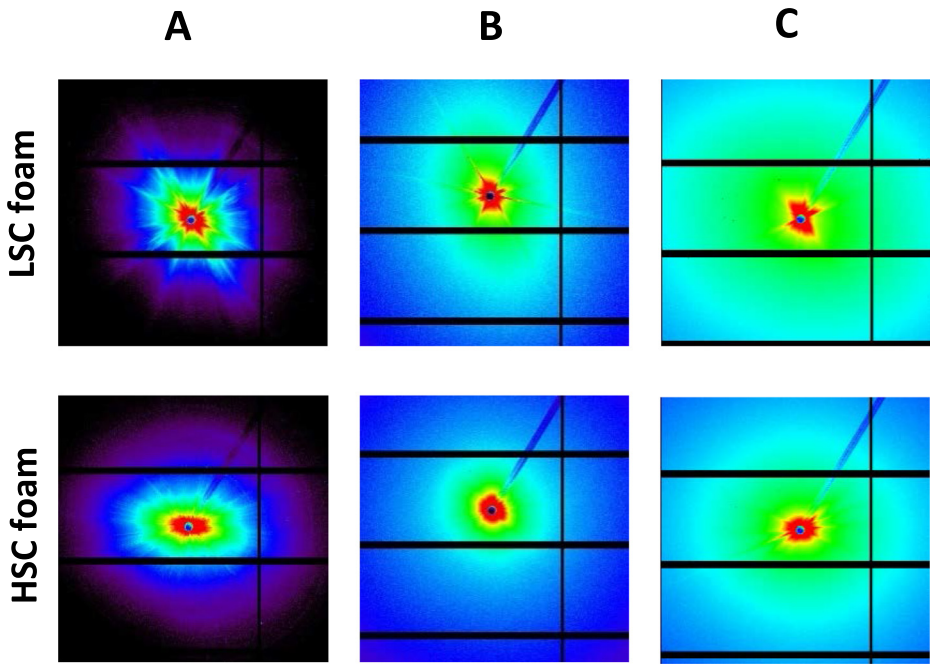

Fig. 4. SAXS measurements of LSC and HSC nanocellulose foams. (A) Dry foam and wet foam in (B) MilliQ water, and (C) 0.9 wt% NaCl. The first row represents the LSC foam while the second row is for HSC foams.

by image analysis, and fiber swelling is dominant when absorption continues to increase although the liquid stain area remains constant. Fig. 6 shows the three different phases of the absorption phenomena by following the size of the liquid stain: wicking (0 to 0.7 s- Phase I); transition (0.7 to 3.8 s- Phase II) and fiber swelling (from 3.8 s- Phase III).

Fluid accommodated by Phase I has been correlated to pore volume in Table 2. The fluid absorbed in phase I of Fig. 3 mainly results from the absorption capacity driven by the pore volume.

Wicking is driven by capillary forces [25] and is mainly characterized by a high initial absorption rate. The inset of Fig. 6 shows that the wicking height is proportional to the square root of time for Phase I, following the Lucas- Washburn equation. As absorption progresses and fiber swelling begins to reduce the dimensions of the inter-fiber pore spaces [26], wicking becomes limited and the transport of liquid through the nanocellulose foam structure relies increasingly on diffusion (Phase III) over capillary action following the transition phase (Phase II) [9]. This results in a reduction in the rate of absorption as seen by the decreasing slope which signals the onset of the transition phase (Phase II).

4.2. Effect of ionic strength on absorption

The nanocellulose foam absorption capacity for the 0.9 wt% NaCl solution is lower than for MilliQ water (Fig. 2). This corroborates the findings of Sultana et al. for different SAPs [10]. The nanocellulose foam contains free mobile ions in its structure that exert an osmotic pressure on the fiber network. A difference in

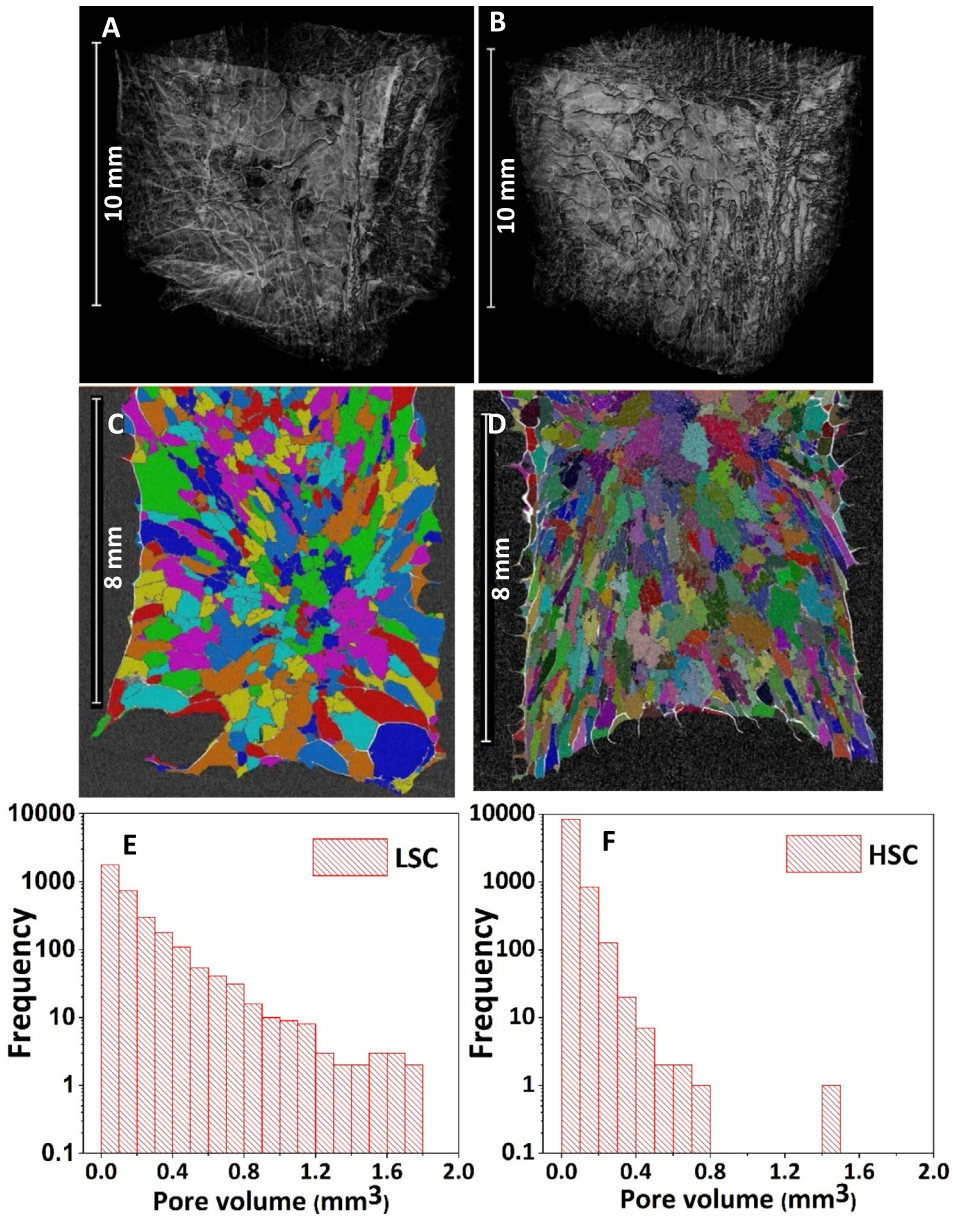

Fig. 5. Structural analysis of nanocellulose foams by X-ray tomography. 3D structure of: (A) LSC foam, (B) HSC foam; XZ planar slice showing separated pore structure of (C) LSC foam, and (D) HSC foam; pore size distribution of (E) LSC and (F) HSC foam.

osmotic pressure between the fiber network and the absorbate creates a driving force for absorption to occur [27]. Addition of salt to the absorbate reduces the osmotic pressure difference and hence reduces the driving force for absorption. The lower absorption capacity in 0.9 wt% NaCl solution than in MilliQ water is also a consequence of charge shielding as increasing the concentration of free ions in the absorbate reduces the interaction of the nanocellulose carboxylate (COO^-) groups with water molecules, therefore decreasing their affinity and absorption propensity [13].

4.3. Effect of surface charge on absorption

4.3.1. Deionised water

The high surface charge foam exhibits slower absorption kinetics than low surface charge foam for MilliQ water. From the absorption experiments, LSC foam achieved 80% of its total absorption capacity within the first 3 s whereas HSC foam only reached 62% in the same time period (Fig. 3A). Similarly, after 30 min of free swelling, LSC foam had achieved 75% of its saturation capacity compared to 66% for HSC foam for MilliQ water (Supplementary Info S1). Image analysis of the liquid stain confirms the slower kinetics of the HSC foam compared to the LSC (Fig. 7A). The slower absorption kinetics and higher saturation capacity indicate that a major part of the absorption capacity of HSC foam results from fiber swelling. The osmotic pressure is increased in HSC foam due to an augmented charge density which facilitates higher fiber swelling in HSC foam compared to LSC foam [28–30].

The slower absorption kinetic of the HSC foam is due to its lower pore size compared to the LSC foam. The HSC foam also has a higher surface charge which improves the efficiency and therefore the extent of fibrillation due to greater electrical repulsion combined with lower hydrogen bonding [24].Thus, HSC foam porosity is lower than that of the LSC foam [31]. As flow resistance from small pores decelerates wicking [32], LSC foams exhibit a higher rate of initial absorption compared to HSC foams.

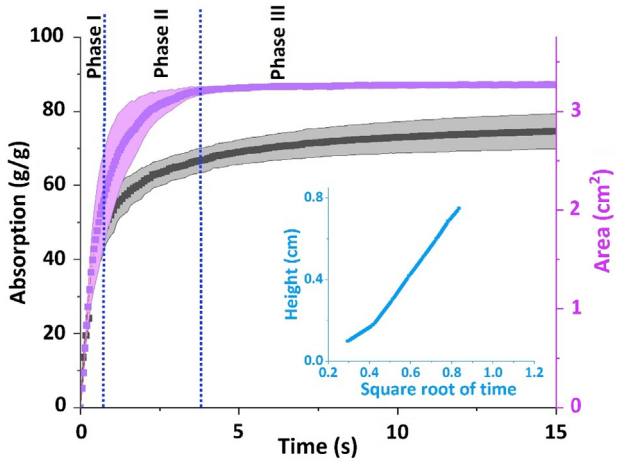

Fig. 6. Effect of wicking and fiber swelling in nanocellulose foam. The black line indicates absorption and the purple represents the area data. The inset shows the relationship between wicking height and time for phase I. The solid line is the average (n = 3), while the shaded zone indicates the range formed by one standard deviation. (For interpretation of the references to color in this figure legend, the reader is referred to the web version of this article.)

4.3.2. 0.9 wt% saline solution

HSC foam exhibits similar absorption kinetics but higher absorption capacity than LSC foam when absorbing a NaCl solution (Fig. 3B). Image analysis confirms that HSC and LSC foams have similar wicking kinetics in a NaCl solution (Fig. 7B). However, the absorption capacity of HSC is higher (Fig. 3B) which means fibre swelling is higher for HSC foam compared to that of LSC for NaCl solution.

5. Conclusion

Nanocellulose based foams are attractive because of their inherent renewability and biodegradability [33]. Nanocellulose foam with different solid concentrations and surface charges have already been developed [13,24]. The swelling of natural polymers, cellulose films and superabsorbents has been previously analysed as a function of pH and ionic strength [28,34–37]. However, the absorption kinetics, the mechanism and the absorption phases for a fast-swelling foam/superabsorbent have not been reported. In this study, the absorption kinetics of superabsorbent nanocellulose foams varying in charge density (controlled with the COO^- concentration) are measured for MilliQ water and 0.9 wt% NaCl solution and the results interpreted in terms of foam structure and absorption mechanism. The absorption kinetics is measured at time frames ranging from a fraction of a second to a few minutes to elucidate the full absorption mechanism and correlate it with foam structure and porosity.

Kinetics and wicking area data both confirm the occurrence of three distinct stages of absorption. These are: 1) wicking, 2) transition and 3) fiber swelling. Wicking is driven by capillary forces and dominates in the first few seconds of absorption. The wicking rate of nanocellulose foams for MilliQ water depends on pore size, as

Table 2
Analysis of pore volume and fluid accommodated by pore volume of the NC foams.

Parameter		Volumetric pore density (mm^3/ mm^3)	Fluid accommodated by pore volume (g/g foam)	Fluid absorbed in phase I (g/g foam)	Percentage of fluid accommodated by pore volume after 5 mins absorption
LSC	MilliQ	0.88	42.7	46.8	52.8
	Saline			41.4	65.8
HSC	MilliQ	0.76	35.8	36.2	41.8
	Saline			34.1	45.3

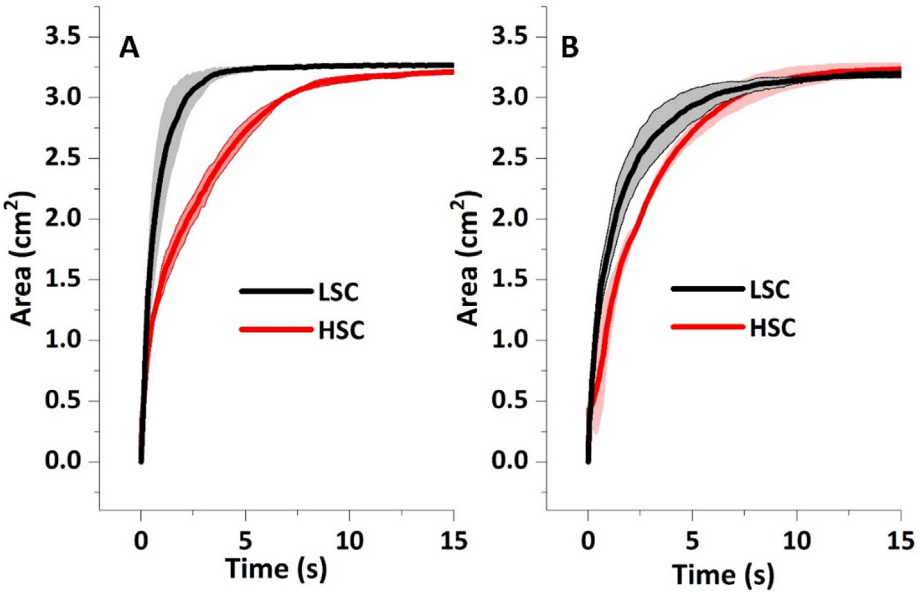

Fig. 7. Effect of surface charge on the stain area of the absorbed fluid over time for LSC and HSC NC foams, for (A) Milli Q water and (B) 0.9 wt% NaCl. The solid line is the average (n = 3), while the shaded zone indicates the range formed by one standard deviation.

evidenced from X-ray computed tomography, with higher rates for foams with larger pore sizes. Wicking is followed by the transition phase, after which fiber swelling dominates the absorption mechanism. A high surface charge (density of COO^- groups) increases fiber swelling [38], which is a slower mechanism than wicking. The slower absorption kinetics of high surface charge fiber foam are therefore due to both smaller pore size and higher concentration of COO^- groups. When absorbing an ionic solution, fiber swelling is reduced due to charge shielding and, as a result, the maximum absorption capacity of nanocellulose foam is decreased. Small Angle X-ray Scattering analysis corroborates this hypothesis by revealing the occurrence of fiber agglomeration in both high and low surface charge nanocellulose foams for the absorption of NaCl solution.

This fundamental absorption study aims to elucidate the initial absorption mechanism of nanocellulose foam. Using these results, performant biosourced and sustainable nanocellulose foams with the desired structure and absorption kinetics can be engineered. These foams can meet the stringent standards and performance criteria for applications such as baby diapers, personal hygiene products or biosensors, and represent a sustainable alternative to petrochemical-based superabsorbent polymers.

CRediT authorship contribution statement

Laila Hossain: Conceptualization, Visualization, Methodology, Investigation, Software, Writing-Original Draft. **Emily Eastman:** Investigation, Softwar. **Monica De Rango:** Investigation, Software. **Vikram Singh Raghuwanshi:** Investigation, Software, Writing-Review & Editing. **Joanne Tanner:** Supervision, Writing- Review & Editing. **Gil Garnier:** Visualization, Supervision, Writing- Review & Editing.

Declaration of Competing Interest

The authors declare that they have no known competing financial interests or personal relationships that could have appeared to influence the work reported in this paper.

Acknowledgment

Financial support was received from Meat and Livestock Australia (MLA) [grant number P.PSH.0890]. The authors acknowledge Stephen Mudie, Nigel Kirby from the SAXS/WAXS beamline at the Australian Synchrotron for the SAXS measurement. Moreover, authors acknowledge ANSTO for the beamtime. The authors also thank Micro-Computed Tomography facilities in University of Melbourne. And thanks to David Mendoza for providing the tempo-periodate oxidized fiber.

Appendix A. Supplementary material

Supplementary data to this article can be found online at https://doi.org/10.1016/j.jcis.2021.05.092.

References

[1] M.J. Zohuriaan-Mehr, K. Kabiri, Superabsorbent polymer materials: a review, Iranian Polymer Journal 17 (6) (2008) 451.
[2] R.M. Barajas-Ledesma, A.F. Patti, V.N. Wong, V.S. Raghuwanshi, G. Garnier, Engineering nanocellulose superabsorbent structure by controlling the drying rate, Colloids Surf. A: Physicochem. Eng. Aspects 600 (2020) 124943.
[3] A. Sawut, M. Yimit, W. Sun, I. Nurulla, Photopolymerisation and characterization of maleylatedcellulose-g-poly (acrylic acid) superabsorbent polymer, Carbohydr. Polym. 101 (2014) 231–239.
[4] M.N. Alam, L. Christopher, Natural Cellulose-Chitosan Crosslinked Superabsorbent Hydrogels with Superior Swelling Properties, ACS Sustain. Chem. Eng. 6 (7) (2018) 8736–8742.
[5] M.I.H. Mondal, Cellulose-based superabsorbent hydrogels, Basel:Springer (2019).
[6] Y. Zhang, T. Nypelö, C. Salas, J. Arboleda, I.C. Hoeger, O.J. Rojas, Cellulose nanofibrils, J. Renewable Mater. 1 (3) (2013) 195–211.
[7] K.J. De France, T. Hoare, E.D. Cranston, Review of hydrogels and aerogels containing nanocellulose, Chem. Mater. 29 (11) (2017) 4609–4631.
[8] L. Soriano, M. Rahman, Wicking Properties of Brassica Fiber in Three Different Growth Stages.(2016).
[9] S. Akinli-Kocak, The influence of fiber swelling on paper wetting.Electronic Theses and Dissertations, 253. (2001).
[10] S. Sultana, M.S. Rahaman, S.M.M. Hasnine, Effect of Salinity on swelling behaviors of superwater absorbent hydrogel prepared from carboxymethyl cellulose/acrylamide blends by gamma radiation, Am. J. Appl. Ind. Chem. 2 (2) (2018) 20–26.
[11] D.R. Schuchard, J.C. Berg, Liquid transport in composite cellulose—superabsorbent fiber networks, Wood Fiber Sci. 23 (3) (2007) 342–357.
[12] M.A. Hubbe, A. Ayoub, J. Daystar, R. Venditti, J. Pawlak, Enhanced absorbent products incorporating cellulose and its derivatives: a review, BioResources. (2013) 6556.
[13] L. Mendoza, L. Hossain, E. Downey, C. Scales, W. Batchelor, G. Garnier, Carboxylated nanocellulose foams as superabsorbents, J. Colloid Interface Sci. 538 (2019) 433–439.
[14] S.R.D. Petroudy, J. Ranjbar, E.R. Garmaroody, Eco-friendly superabsorbent polymers based on carboxymethyl cellulose strengthened by TEMPO-mediated oxidation wheat straw cellulose nanofiber, Carbohydr. Polym. 197 (2018) 565–575.
[15] F. Nnadi, C. Brave, Environmentally friendly superabsorbent polymers for water conservation in agricultural lands, J. Soil Sci. Environ. Manage. 2 (7) (2011) 206–211.
[16] J. Patiño-Masó, F. Serra-Parareda, Q. Tarrés, P. Mutjé, F.X. Espinach, M. Delgado-Aguilar, TEMPO-oxidized cellulose nanofibers: a potential bio-based superabsorbent for diaper production, Nanomaterials 9 (9) (2019) 1271.
[17] C. Demitri, R. Del Sole, F. Scalera, A. Sannino, G. Vasapollo, A. Maffezzoli, L. Ambrosio, L. Nicolais, Novel superabsorbent cellulose-based hydrogels crosslinked with citric acid, J. Appl. Polym. Sci. 110 (4) (2008) 2453–2460.
[18] P.W. Brodin, H. Theliander, Absorbent materials based on kraft pulp: Preparation and material characterization, BioResources 7 (2) (2012) 1666–1686.
[19] F.W. Brodin, Y. Sonavane, H. Theliander, Preparation of absorbent foam based on softwood kraft pulp: advancing from gram to kilogram scale, BioResources 8 (2) (2013) 2099–2117.
[20] A. Olad, F. Doustdar, H. Gharekhani, Fabrication and characterization of a starch-based superabsorbent hydrogel composite reinforced with cellulose nanocrystals from potato peel waste, Colloids Surf., A 601 (2020) 124962.
[21] T. Saito, S. Kimura, Y. Nishiyama, A. Isogai, Cellulose nanofibers prepared by TEMPO-mediated oxidation of native cellulose, Biomacromolecules 8 (8) (2007) 2485–2491.
[22] D.J. Mendoza, C. Browne, V.S. Raghuwanshi, G.P. Simon, G. Garnier, One-shot TEMPO-periodate oxidation of native cellulose, Carbohydr. Polym. 226 (2019) 115292.
[23] T. Fekete, J. Borsa, E. Takács, L. Wojnárovits, Synthesis of carboxymethylcellulose/starch superabsorbent hydrogels by gamma-irradiation, Chem. Cent. J. 11 (1) (2017) 46.
[24] D.J. Mendoza, L. Hossain, C. Browne, V.S. Raghuwanshi, G.P. Simon, G. Garnier, Controlling the transparency and rheology of nanocellulose gels with the extent of carboxylation, Carbohydr. Polym. 245 (2020) 116566.
[25] Z. Liu, X. He, J. Han, X. Zhang, F. Li, A. Li, Z. Qu, F. Xu, Liquid wicking behavior in paper-like materials: mathematical models and their emerging biomedical applications, Microfluid Nanofluid 22 (11) (2018) 132.
[26] A. Patnaik, R.S. Rengasamy, V.K. Kothari, A. Ghosh, Wetting and Wicking in Fibrous Materials, Text. Prog. 38 (1) (2006) 1–105.
[27] M. Elliott, Superabsorbent polymers. Product development scentist for SAP. BASF Aktiengesellschaft ss, 13 2004.
[28] S. Fält, L. Wågberg, E.-L. Vesterlind, Swelling of model films of cellulose having different charge densities and comparison to the swelling behavior of corresponding fibers, Langmuir 19 (19) (2003) 7895–7903.
[29] S. Hanhikoski, I. Solala, P. Lahtinen, K. Niemelä, T. Vuorinen, Fibrillation and characterization of lignin-containing neutral sulphite (NS) pulps rich in hemicelluloses and anionic charge, Cellulose (2020).
[30] F.L. Buchholz, A.T. Graham, Modern superabsorbent polymer technology. Wiley & Sons, Inc, 605 Third Ave, New York, NY 10016, USA, 1998. 279.1998.
[31] M. Wakabayashi, S. Fujisawa, T. Saito, A. Isogai, Nanocellulose film properties tunable by controlling degree of fibrillation of TEMPO-oxidized cellulose, Front. Chem. 37 (8) (2020).
[32] S. Ahmed, M.-P.N. Bui, A. Abbas, Paper-based chemical and biological sensors: engineering aspects, Biosens Bioelectron. 77 (2016) 249–263.
[33] D. Klemm, E.D. Cranston, D. Fischer, M. Gama, S.A. Kedzior, D. Kralisch, F. Kramer, T. Kondo, T. Lindström, S. Nietzsche, Nanocellulose as a natural source for groundbreaking applications in materials science: Today's state, Mater. Today 21 (7) (2018) 720–748.
[34] K. Kabiri, M. Zohuriaan-Mehr, Superabsorbent hydrogel composites, Polym. Adv. Technol. 14 (6) (2003) 438–444.
[35] G.F. de Lima, A.G. de Souza, D.d.S. Rosa, Nanocellulose as reinforcement in carboxymethylcellulose superabsorbent nanocomposite hydrogels, Macromol. Symp. 394 (1) (2020) 2000126. Wiley Online Library.

[36] N. Deghiedy, Synthesis and Characterization of Super absorbent Hydrogels Based on Natural Polymers Using Ionizing Radiations. 2010, Faculty of Science Al-Azhar University (Girls) Cairo In the partial fulfillment for M. Sc. Degree in Chemistry (Organic Chemistry) Submitted by Noha Mohamed Abd El-Salam Deghiedy B. Sc. of Science (Special Chemistry) Faculty of Science, Al-Azhar University.

[37] D. Das, P. Prakash, P.K. Rout, S. Bhaladhare, Synthesis and characterization of superabsorbent cellulose-based hydrogel for agriculture application, Starch - Stärke 73 (1-2) (2021) 1900284.

[38] M. Mayr, R. Eckhart, H. Winter, W. Bauer, A novel approach to determining the contribution of the fiber and fines fraction to the water retention value (WRV) of chemical and mechanical pulps, Cellulose 24 (7) (2017) 3029–3036.